

Relevance of relative sea surface temperature for tropical rainfall interannual variability

Takeshi Izumo^{1,2}, Jérôme Vialard¹, Matthieu Lengaigne^{1,2} and Iyyappan Suresh³

¹ Institut de Recherche pour le Développement, Sorbonne Universités (UPMC, Univ Paris 06)-CNRS-IRD-MNHN, LOCEAN Laboratory, IPSL, Paris, France

² formerly at Indo-French Cell for Water Sciences, IISc-NIO-IITM-IRD Joint International Laboratory, NIO, Goa, India

³ CSIR-National Institute of Oceanography, Goa

Abstract

The coupling between Sea surface temperature anomalies (SST') and rainfall is an important driver of tropical climate variability. Observations however reveal inconsistencies, such as decreased convective rainfall in regions with positive SST' in the tropical Indian and Atlantic Oceans during and after El Niño Southern Oscillation (ENSO) events. The upper troposphere warms during El Niño events, stabilizing the atmosphere. SST' only account for the influence of the surface. Using theoretical arguments, we show that relative SST anomalies (RSST'; defined as SST' minus their tropical mean), by also accounting for the influence of upper tropospheric signals on stability, explain tropical convection interannual variations better than SST' in observations and climate models. This relation further improves when RSST' is weighted by the precipitation climatology to account for low and high-precipitation regimes. RSST' is thus a useful indicator to understand ENSO teleconnections, and interactions between modes of tropical climate variability.

Key points

- Relative Sea Surface Temperature anomalies (RSST') are defined as SST anomalies minus their tropical mean
- RSST', rather than SST', drive tropical convection interannual variability, especially when weighted by climatological precipitation
- RSST' account for the ENSO-induced upper-tropospheric temperature signal influence on stability, and explain ENSO teleconnections better

Keywords:

Air-sea coupling, relative Sea Surface Temperature (RSST), interannual variability, El Niño Southern Oscillation (ENSO), teleconnections, tropical rainfall and precipitation, deep atmospheric convection, atmospheric stability.

Plain language summary

Rainfall is an important driver of coupled air-sea climate variability in tropical regions, through its influence on atmospheric motions. Sea surface temperature anomalies influence tropical rainfall, as a warm anomaly is expected to destabilize the atmosphere, yielding a rising motion and increased rainfall. Decreased rainfall however sometimes occur over positive sea surface temperature anomalies, notably during El Niño events, because these events tend to warm the upper atmosphere in the entire tropics, hence stabilizing the atmosphere and inhibiting rainfall. We show that the relative sea surface temperature, defined as the sea surface temperature minus its average over the tropical oceans, explains precipitation anomalies better than sea surface temperature. Relative sea surface temperature is thus a simple and powerful indicator to better understand year-to-year climate variability, notably El Niño Southern Oscillation influence on rainfall in the Atlantic and Indian Oceans, and its interactions with other tropical ocean-atmosphere coupled modes.

1. Introduction

Tropical rainfall variability has strong socio-economic and environmental impacts, notably in the vulnerable, heavily populated, tropical regions (e.g. Gadgil and Gadgil 2006; Boko et al. 2007). Convective rainfall, which accounts for most of the tropical rainfall, plays a key role in tropical atmospheric motions. For instance, the latent heat release due to deep-atmospheric convection over the Indo-Pacific warm pool energizes the Walker Circulation (e.g. Gill 1980). A necessary condition for deep atmospheric convection to occur is a Sea Surface Temperature (hereafter, SST) exceeding $\sim 28^{\circ}\text{C}$ (e.g. Gadgil et al. 1984; Graham and Barnett 1987), as it destabilizes the atmosphere. The link between SST and convective interannual anomalies plays a key role in shaping tropical climate variability. During El Niño Southern Oscillation (ENSO) events, for instance, positive SST anomalies induce enhanced convection in the central Pacific, thereby yielding westerly wind anomalies and an equatorial Pacific oceanic response that will further strengthen the initial SST anomalies. This positive feedback that allows the growth of El Niño events is known as the Bjerknes feedback. It also plays a key role in the development of the Indian Ocean Dipole (IOD; e.g. Saji et al. 1999) and Atlantic Niño (e.g. Merle 1980), which are intrinsic climate modes in the Indian and Atlantic Oceans, respectively.

This crucial SST-convection relation is however far from perfect, as illustrated on Figure 1. Figure 1a shows the lag-correlation between the El Niño peak intensity and the tropical Indian Ocean SST and rainfall interannual anomalies. The Indian Ocean tends to warm during and after El Niño events, a response to ENSO referred to as the Indian Ocean Basin Mode (IOBM; e.g. Klein et al. 1999) and related “capacitor effect” (Xie et al. 2009). This warming is the result of the eastward shift in the Walker circulation, which induces increased subsidence and downward solar radiation (e.g. Lau and Nath 2003) and reduced evaporation over the Indian Ocean (e.g. Ohba and Ueda 2005). This Indian Ocean warming however does not enhance regional rainfall from September to February, but rather leads to negligible or negative rainfall anomalies. A similar mismatch between SST and convective anomalies occurs over the Tropical Atlantic. Reduced winds and evaporation also induce a tropical North Atlantic (TNA) warming during the years that follow El Niño events (e.g. Garcia-Serrano et al. 2017), in association with negative rainfall anomalies (Fig. 1b). The relation between SST and convective anomalies is hence not always consistent with the simple principle that warmer SST destabilizes the atmosphere and increases rainfall over the tropical Indian and Atlantic Oceans during ENSO events. This mismatch between convective and SST anomalies is likely due to two factors.

First, atmospheric stability is not only determined by surface properties, but also by anomalies in the upper troposphere, as demonstrated by Neelin and Held (1987). Those authors defined gross moist stability (GMS) as the difference of Moist Static Energy (MSE) between the surface and upper troposphere and showed that precipitation (P) tends to be inversely proportional to GMS ($P \approx F/GMS$, F being a constant). Based on partly-similar arguments, studies (e.g. Vecchi and Soden 2007; Vecchi et al. 2008; Ramsay and Sobel 2011) aimed at understanding the tropical cyclones response to climate change showed that the tropical cyclones potential intensity (PI) rather depends of the *relative* SST (hereafter RSST), defined as the local SST minus its tropical mean (denoted $\langle SST \rangle$). The underlying idea is that RSST can be used as a proxy for changes in atmospheric stability (and hence tropical cyclones) in a warming world. Temperature in the upper tropical troposphere is relatively homogenous, due to the fast ($\sim 1-2$ months) adjustment timescale of equatorial waves in the free atmosphere (e.g. Sobel and Bretherton 2000; Chiang and Sobel 2002): this is the commonly-used Weak Tropospheric Gradient (WTG) approximation (Sobel et al. 2001; Ramsay and Sobel 2011). Hence, since the tropical troposphere tends to follow the moist adiabatic vertical profile (e.g. Stone and Carlson 1979), the upper troposphere will tend to warm uniformly under climate change, so that what matters for changes in atmospheric stability (and hence tropical cyclones) are deviations from the mean surface warming, i.e. RSST. Johnson and Xie (2010) used this property to explain that the “threshold” for deep atmospheric convection will increase at the same rate as the tropical mean SST in response to anthropogenic climate change. RSST has to date mostly been used in the global warming context, for instance to understand the spatial patterns of changes in tropical cyclones (as afore-mentioned), in the hydrological cycle (e.g. Xie et al. 2010), and to define ENSO events (Williams and Patricola 2018) and their convective signature (Johnson and Kosaka 2016) in a warming world. RSST also allows isolating the ENSO and IOD signals in the context of global cooling induced by tropical explosive volcanic eruptions (Khodri et al. 2017, Izumo et al. 2018). RSST is finally useful for characterizing the influence of the equatorial Pacific bias in climate model on the Walker Circulation and on ENSO (Bayr et al. 2018, 2019ab). While the above studies largely applied the RSST concept in a global warming/cooling context, Johnson and Xie (2010) remarked that it also seems to explain year-to-year variations of the SST threshold for tropical convection in the Coupled Model Intercomparison Project (CMIP) database (cf. discussion of their figure 2b). This suggests that the RSST concept can also be used to account for the effect of variations in upper tropospheric temperature on stability at the interannual timescale. The entire tropical troposphere indeed tends to warm (cool) during and after El Niño (La Niña) events (Fig. 1cde), increasing (decreasing) the atmospheric stability. The better agreement in Fig. 1ab between the Indian Ocean or Atlantic basin-averaged precipitation and RSST anomalies (hereafter RSST’), than with SST

anomalies (hereafter SST'), suggest that the RSST concept can also be used at the interannual timescale. Our first objective in this paper is to formally show why RSST' controls atmospheric stability at interannual timescale (section 2), and to demonstrate that precipitation and convection interannual anomalies are better explained by RSST' than by SST' (section 4).

A second possible cause for mismatches between SST and rainfall anomalies, e.g. on Figure 1a,b, is the non-linearity of the SST-precipitation relationship. As already noted, tropical deep convection indeed occurs above $\sim 28^\circ\text{C}$ in the present climate (e.g. Gadgil et al. 1984; Jauregui and Takahashi 2017). This implies that SST variations mostly influence rainfall in climatologically-high SST regions (e.g. He et al. 2018). Previous studies (Sobel et al. 2002; Flannaghan et al. 2014, Flueglstaler et al. 2015) have defined a tropical mean Precipitation-weighted (or "rainy") SST to take this effect into account. The simple idea is to give more weight to SST in regions where it rains more. Because we aim at explaining local rainfall anomalies, our second objective in this paper will be to test if a weighting of the RSST by the precipitation climatology further improves its agreement with precipitation/convection by implicitly accounting for the climatological SST distribution.

In section 2, we develop theoretical arguments to explain why RSST' should be a proxy of interannual precipitation anomalies, especially when weighted by climatological precipitation. In section 3, we briefly present the data and methods used (described in detail in the online supplementary material text S5). In section 4, we first demonstrate that RSST' is a better proxy of tropical precipitation anomalies than SST', because they integrate the effect of the upper-tropospheric temperature anomalies on the atmospheric stability, in particular in the Atlantic and Indian Oceans and around the maritime continent during ENSO events. We will then define a climatological Precipitation-weighted RSST' (PcRSST'), and show that it performs even better for explaining anomalous precipitation patterns. We discuss our results - strengthened by analyses of 36 CMIP models in the online supplementary material - in section 5, including implications for a better understanding of interactions between modes of tropical climate variability.

2. RSST as a proxy of atmospheric stability

Here we summarize the main steps of our theoretical demonstration explaining why gross moist stability (GMS) and precipitation interannual anomalies P' ($P' = P - \bar{P}$, with the overbar denoting the monthly seasonal cycle) respond to RSST' (see online supplementary material texts S1 and S2 for a complete derivation and more thorough discussion of the approximations involved). GMS is defined as:

$$\text{GMS} = m_t - m_s$$

where the t and s subscripts respectively denote the upper troposphere (300 hPa level, e.g. Fueglistaler et al. 2015) and surface, m is the Moist Static Energy (MSE; $m = s + L_v q = C_p T + g z + L_v q$ where s is the dry static energy, L_v the latent heat of vaporization, q the specific humidity, C_p the specific heat at constant pressure, T the temperature, g the gravitational constant and z the altitude. The tropical atmosphere approximately follows the moist adiabatic lapse rate (Stone and Carlson 1979), so that $\langle m_t \rangle' = \langle m_s \rangle'$, where $\langle \rangle$ denotes the 20°N-20°S tropical mean (cf. Supplementary text S5A discussing this choice). The upper troposphere is almost dry, and its MSE hence mainly depends on temperature: $m_t \approx s_t = C_p T_t + g z_t \approx (C_p + R/M_{air}) T_t$, where R is the ideal gas constant and M_{air} the air molar mass. Finally, T_t is rather uniform across the tropical band (WTG approximation; Sobel et al. 2001), so that $m_t' \approx \langle m_t \rangle'$. Given all these approximations, the GMS anomalies are given by $GMS' \approx \langle m_s' \rangle - m_s'$.

If we assume an almost constant relative humidity (typically around 80% in the tropics), and a 7% change in specific humidity q_s per °C of SST change (linearization of Clausius-Clapeyron), then $m_s' = C_p T_s' + L_v q_s' \approx (C_p + 0.07 L_v \bar{q}_s) T_s'$, i.e. MSE' is proportional to SST'. Therefore, to the first order, $GMS' \approx (C_p + 0.07 L_v \bar{q}_s) (\langle T_s' \rangle - T_s')$. As $RSST' = T_s' - \langle T_s' \rangle$, we obtain:

$$GMS' \approx -(C_p + 0.07 L_v \bar{q}_s) RSST'$$

Finally, exploiting the theoretical relation between GMS and precipitation derived by Neelin and Held (1987), we obtain:

$$P' \approx RSST' \bar{P} (C_p + 0.07 L_v \bar{q}_s) / \overline{GMS}$$

I.e., precipitation interannual anomalies should be proportional to RSST'. The proportionality constant depends of the climatological mean state, and is in particular proportional to \bar{P} , and hence expected to be larger in regions of high climatological precipitation and SST.

In this section, we have shown that RSST' should be a proxy of tropical precipitation interannual anomalies, in particular when weighted by climatological precipitation. This derivation nonetheless involved several strong approximations (for instance the upper tropospheric signal is not completely homogeneous, Fig. 1d). Section 4 will however demonstrate that RSST' and Pc-RSST' are indeed better proxies of tropical precipitation and convection interannual anomalies, hence justifying our strong assumptions *a posteriori*.

3. Data and methods

We only give a brief summary of our data and methods here, with a comprehensive description in the online supplementary material. We use the OISSTv2 SST product (Reynolds et

al. 2002), NCEP2 reanalysis (Kanamitsu et al. 2002) for temperature at 300 hPa and NOAA Climate Data Record (CDR) Outgoing Longwave Radiation (OLR; Hai-Tien Lee and NOAA CDR Program 2018) as a proxy for deep atmospheric convection, and CMAP1 precipitation (Xie and Arkin 1997). All the analyses are performed on monthly anomalies relative to the mean seasonal cycle, over the November 1981 to 2018 period. The anomalies are smoothed to remove unwanted intraseasonal frequencies prior to analysis. The results are robust when no detrending or smoothing is applied (cf. Supplementary Figure S2). We use classical indices of the interannual tropical climate variability, based on average SST anomalies: the Niño3.4 index for ENSO, Dipole Mode Index (DMI) for the IOD and the Atl3 index for the Atlantic Niño.

4. Results

Figure 2a shows the correlation between precipitation and local SST'. There is a positive correlation, often above 0.4 (and up to above 0.8 in the central equatorial Pacific), in most rainy regions in the tropics, illustrating the tendency for positive SST' to destabilize the atmosphere and induce more convective rainfall (and vice-versa for negative SST'). This relation is particularly strong in the central equatorial Pacific and on the southern flank of the Pacific inter-tropical convergence zone (ITCZ) due to the strong ENSO signal there. At timescales longer than the intraseasonal one, this relationship illustrates the response of atmospheric deep convection to SST' (e.g. Gadgil et al. 1984, Graham and Barnett 1987), except in dry, subsident regions where cloud negative radiative feedbacks can dominate (e.g. He et al. 2018). Overall, SST' hence explain a significant part of the deep convection interannual variability in tropical rainy regions.

Our first objective in this paper is to test the added value of RSST' for explaining tropical convection interannual variability. Figure 2b shows the same analysis as Figure 2a, but based on RSST', and panel c shows the differences between the two panels. This figure indicates that RSST' is a better proxy of convection interannual variability over tropical rainy regions than SST'. This improvement is particularly evident over the warm-pool areas, i.e. over the western equatorial Atlantic, the central and eastern equatorial Indian Ocean, the maritime continent and the western Pacific where correlation increases by up to ~ 0.35 (Fig. 2c). The improvement is even better (up to ~ 0.5) when using a better-observed deep atmospheric convection proxy (OLR; Online supplementary material; Fig. S1). A qualitatively similar improvement is also evident when performing similar analyses in the CMIP5 (IPCC 2013) database (with obviously some differences related notably to models typical climatological biases; Fig. 2d; Supplementary Fig. S3, Fig. S4, and texts S3 and S4). Conversely, RSST' do not perform better than SST' to explain rainfall interannual variations over the central and eastern equatorial Pacific.

Let us now discuss the reasons for this improved RSST' performance. As mentioned earlier, RSST' encapsulate the effect of the upper tropospheric temperature anomalies on gross moist stability, while SST' do not. Those upper tropospheric temperature anomalies are quite uniform across the tropical band (Fig. 1d), and strongly correlated to the tropical-mean SST'(Fig. 1c,e), and to ENSO signal with a 1-2 months time lag (Fig. 1c). The tropical mean SST' component of the RSST' expression hence largely captures the stabilizing (destabilizing) effect of the upper tropospheric warming (cooling) on the atmosphere during El Niño (La Niña) events. In the Pacific, this effect is small relative to the much larger effect of SST'. This explains the similar performance of SST' and RSST' in the central and eastern Pacific regions. The northern half of the South Pacific Convergence Zone (SPCZ) is the only region showing a slightly degraded performance of RSST'(Fig. 2c), most likely because ENSO-related circulation anomalies (e.g. Vincent et al. 2011) also influence rainfall variations in this region. On the other hand, the improved performance of RSST' over the Indian and Atlantic oceans and maritime continent suggests that the ENSO-induced tropospheric temperature signals play a relatively strong role in controlling the atmospheric stability interannual variations there. Below, we examine this by investigating the ENSO teleconnection patterns to the Atlantic and Indian Oceans in terms of SST', RSST' and precipitation anomalies (Fig. 3abcd).

For ENSO-related SST', in boreal fall (September to November) prior to an El Niño peak, there is a marked IOD signal in the Indian Ocean (Fig. 3a), due to the tendency of the IOD to phase-lock to ENSO (e.g. Annamalai et al. 2003, Ohba and Ueda 2005). By the following spring (March to May), the IOD signal is replaced by a clear IOBM warming signal (Fig. 3b). In the Atlantic, the weak Atlantic Niña tendency in fall (Fig. 3a) progressively evolves into a Tropical North Atlantic warming (Fig. 3b), which peaks the following spring (e.g. Taschetto et al. 2016). However, these Indo-Atlantic SST' do not match the observed pattern of precipitation anomalies very well (Fig. 3a,b). The Indo-Atlantic uncentered pattern correlation between ENSO-related precipitation and SST' is only 0.52 in fall (Fig. 3a) and 0.21 in the following spring (Fig. 3b). For instance, in the Indian Ocean, positive SST' in the Bay of Bengal are associated with negative precipitation anomalies; notably in boreal fall, these negative precipitation anomalies are much broader than the underlying negative SST' of the IOD east pole, relatively weak and confined. In the Atlantic, there are significant decreased rainfall anomalies along the ITCZ in spring, in the absence of clear negative SST'(Fig. 3b).

RSST' is negatively offset relative to SST' during an El Niño (Fig. 3cd) due to the removal of the positive tropical mean SST' (Fig. 1). This offset captures the stabilizing effect of the upper tropospheric warming over the Atlantic and Indian Oceans during El Niño events. As a result,

precipitation anomalies spatial patterns match those of RSST' better than those of SST'. Pattern correlations indeed increase from 0.52 to 0.65 in fall (Fig. 3a,c), from 0.21 to 0.54 in the following spring (Fig. 3b,d), and even from -0.02 to +0.52 in winter (Online supplementary material figure S5). The decreased rainfall over the Bay of Bengal, increased rainfall in the southwestern Indian Ocean in spring, or decreased rainfall along the Atlantic ITCZ all match the RSST pattern better than that of SST. RSST not only explains precipitation anomalies better than SST, but also the near surface wind anomalies they induce. For instance, the correlation between the DMI eastern pole index and zonal equatorial Indian Ocean wind anomalies (in boreal fall during IOD peak season) increase from 0.68 to 0.83, or that between the Atl3 index and equatorial Atlantic winds (in spring-summer during Atlantic Nino peak season) from 0.8 to 0.89 (both improvement being significant at the 95% confidence level). Overall, this illustrates that the effect of ENSO on upper tropospheric temperature need to be considered in addition to local SST' to explain the rainfall and surface wind interannual anomalies in the tropical Indian and Atlantic oceans.

Even though RSST' exhibits a better pattern agreement with precipitation anomalies than SST', the agreement can be further improved. For instance, dry anomalies above the IOD eastern pole only extend down to 10°S, while the broad negative RSST' extends further south (Fig. 3c). Similarly, the Atlantic exhibits a very broad tropical negative RSST', while the rainfall decrease is confined near the equator. In both cases, the precipitation anomalies tend to be more concentrated in the regions of highest climatological SST and rainfall. This brings us to our second objective: to test the potential added value of weighting RSST' by the precipitation climatology as a proxy of convective precipitation interannual variability. We define $PcRSST' = Pc \times RSST' / \langle Pc \rangle$, where Pc is the seasonally-variable precipitation climatology. The $PcRSST'$ pattern even better matches that of rainfall anomalies in the eastern Indian Ocean and Atlantic (Fig. 3e). The IOD in fall is actually rather an east IO "monopole" than a dipole in terms of $PcRSST'$ and precipitation, and the Atlantic meridional dipole in spring as well is almost an equatorial monopole. This better match results in an Indo-Atlantic pattern correlation improvement from 0.65 to 0.79 in boreal fall and 0.54 to 0.60 in the following spring. $PcRSST'$ is also very relevant during the ENSO peak in winter, improving the Indo-Pacific pattern correlation from 0.52 to 0.67 (Online supplementary material Fig. S5). As a comparison, using SST weighted by precipitation climatology, $PcSST$, leads only to a slight improvement as compared to SST, weaker than RSST, and hence clearly weaker than $PcRSST'$ (not shown). Furthermore, El Niño and La Niña composites equivalent to figure 3 confirm that $PcRSST'$ and RSST match Indian Ocean and Atlantic precipitation anomalies better than SST for both ENSO phases (Supplementary Figures S6 and S7), i.e. that the nonlinear relation between surface temperature and precipitation does not affect the superior performance of RSST'.

Overall, this analysis demonstrates that PcRSST is a very good proxy of the precipitation interannual anomalies over the Indian and Atlantic oceans, because it encapsulates both the surface and the upper tropospheric influences on atmospheric stability, and takes into account some of the non-linear dependency of rainfall to SST, with the strongest rainfall response at high SST.

5. Discussion

Earlier studies have introduced RSST (simply defined as SST minus its tropical mean) as a driver of the changes in tropical atmospheric deep convection in the context of climate change. Using a theoretical derivation, we show that interannual anomalies of precipitation should also be proportional to RSST interannual anomalies, with a larger proportionality coefficient in climatologically-high rainfall regions. Using observations - and CMIP models (see also online supplementary material) - we show that RSST explains deep atmospheric convection anomalies better than SST, because they encapsulate the effects of upper-tropospheric temperature anomalies on stability changes. This is particularly relevant during ENSO events, because El Niño (La Niña) uniformly warms (cools) the upper troposphere, thereby stabilizing (destabilizing) the tropical atmosphere. In CMIP models, this added value of RSST is thus larger in the model having larger ENSO amplitude (supplementary Fig. S4), and is projected to remain robust in the future (online supplementary material texts S3 and S4).

Weighting RSST by the precipitation climatology (PcRSST) further improves the consistency with interannual rainfall anomalies, by accounting for the non-linearity in the SST-rainfall relation, with tropical rainfall mostly occurring above a SST threshold of $\sim 28^{\circ}\text{C}$ in the current climate (i.e. above a RSST threshold of $\sim 1^{\circ}\text{C}$; Johnson and Xie 2010). PcRSST can also help us in understanding the asymmetries of El Niño and La Niña teleconnections (supplementary figures S6 and S7). RSST/PcRSST are thus easy-to-compute, physical variables (and thus proxies) driving tropical precipitation/convection anomalies (and their dynamical response, notably surface wind). They account both for the effects of surface and upper-tropospheric temperature anomalies, e.g. in the context of the pan-tropical upper tropospheric signals induced by ENSO, but also in those associated with global climate change (e.g. Vecchi and Soden 2007; Vecchi et al. 2008; Johnson and Xie 2010) or tropical explosive volcanic eruptions (Khodri et al. 2017). RSST should thus be used, instead of SST (or at least complementary to SST), to define coupled climate modes indices (e.g. Atl3, DMI east pole and Niño3.4 RSST) that are more dynamically consistent with precipitation/wind. Such RSST use should become even more essential in the increasing trend context due to global anthropogenic warming (online supplementary material text S4).

Our results have implications for the studies that investigate remote effects of SST anomalies in, e.g. the Atlantic or Indian Ocean, on the evolution of ENSO events, both at interannual and decadal timescales (RSST concept being a priori valid for both). Such studies often investigate teleconnections to winds over the Pacific using atmospheric (or coupled) general circulation models sensitivity experiments forced by SST anomalies applied only in e.g. the Atlantic or Indian Ocean (e.g. Annamalai et al. 2005; Ding et al. 2012; Luo et al. 2012; Santoso et al. 2012; Ham et al. 2013; Chikamoto 2014; McGregor et al. 2014; Dayan et al. 2015). While this strategy is correct for SST anomalies that are independent of ENSO, it may give a biased result for climate modes that are tightly associated with ENSO. The IOBM and TNA are for instance systematically forced by an ENSO signal and will hence always involve an upper tropospheric temperature signal. A numerical experiment forced by SST anomalies only applied in the Indian Ocean or Atlantic will miss most of the upper tropospheric signal, and hence not accurately estimate the actual regional precipitation anomalies and their remote circulation response over the Pacific. In other words, since RSST' explains precipitation (and wind) anomalies related to e.g. the IOD, the IOBM and TNA better than SST' (Fig. 3), it would be more appropriate to apply RSST rather than SST anomalies in the Atlantic and Indian oceans to study their remote effects on the Pacific.

RSST could also allow revisiting interactions between tropical climate modes (e.g. Cai et al. 2019). Many studies have for instance questioned the interdecadal stability of the ENSO influence on tropical Atlantic SST (e.g. Rodriguez-Fonseca et al. 2009; Ding et al. 2012). The correlation between Nino3.4 and Atl3 SST' in April–June (Atlantic Nino peak season) is indeed significant at the 95% level over the 1981-2001 period ($r=0.58$) but not over 1998-2018 ($r=0.39$). This correlation is significant over both periods when computed from RSST' (0.70 and 0.59; in fact there is a more robust correlation using RSST' over the entire historical period). This suggests that the remote influence of ENSO on Atlantic rainfall and the associated wind anomalies (i.e. the ENSO teleconnection to the Atlantic) has remained quite stable over recent decades. What has not remained stable is the tendency of this atmospheric circulation change to induce a SST anomaly (Chang et al. 2006). This provides new clues to investigate the relations between ENSO and the Atlantic. Similarly, additional analyses based on RSST' (not shown) highlight the dominant role of the IOD eastern pole (actually a RSST monopole; Figs 3, S5 and S6) in generating a rainfall response over the IO, and related wind responses over the equatorial IO and western Pacific. The RSST' hence offers interesting perspectives to study the IOD influence on ENSO (e.g. Izumo et al. 2010, 2013, 2016; Jourdain et al. 2016; Wieners et al. 2017).

Acknowledgements. :

We thank the two reviewers, Dr. Thomas Bayr and an anonymous one, for their constructive comments on this work. We thank Institut de Recherche pour le Développement (IRD) and CSIR-National Institute of Oceanography (CSIR-NIO) for their continuous supports. This work was mainly done while TI was a visiting scientist under IRD funding at CSIR-NIO. JV thanks IRD for funding regular visits to CSIR-NIO and CSIR-NIO for his “Adjunct Scientist” position. This work has also been funded by the ARISE ANR project (ANR-18-CE01-0012). We thank NOAA for making the FERRET software available. All data for this paper is properly cited and referred to in the reference list.

References

- Adames, Á. F., & Wallace, J. M. (2017). On the tropical atmospheric signature of El Niño. *Journal of the Atmospheric Sciences*, 74(6), 1923-1939.
- Annamalai, H., Murtugudde, R., Potemra, J., Xie, S. P., Liu, P., & Wang, B. (2003). Coupled dynamics over the Indian Ocean: Spring initiation of the zonal mode. *Deep Sea Research Part II: Topical Studies in Oceanography*, 50(12-13), 2305-2330.
- Annamalai, H. S. P. X., Xie, S. P., McCreary, J. P., & Murtugudde, R. (2005). Impact of Indian Ocean sea surface temperature on developing El Niño. *Journal of Climate*, 18(2), 302-319.
- Bayr, T., M. Latif, D. Dommenges, C. Wengel, J. Harlaß, and W. Park, 2018: Mean-state dependence of ENSO atmospheric feedbacks in climate models. *Clim. Dyn.*, 50, 3171-3194, doi:10.1007/s00382-017-3799-2.
- Bayr, T., C. Wengel, M. Latif, D. Dommenges, J. Lübbecke, and W. Park, 2019a: Error compensation of ENSO atmospheric feedbacks in climate models and its influence on simulated ENSO dynamics. *Clim. Dyn.*, 53, 155-172, doi:10.1007/s00382-018-4575-7.
- Bayr, T., D. I. V. Domeisen, and C. Wengel, 2019b: The effect of the equatorial Pacific cold SST bias on simulated ENSO teleconnections to the North Pacific and California. *Clim. Dyn.*, 1-19, doi:10.1007/s00382-019-04746-9.
- Bellenger, H., Guilyardi, É., Leloup, J., Lengaigne, M., & Vialard, J. (2014). ENSO representation in climate models: from CMIP3 to CMIP5. *Climate Dynamics*, 42(7-8), 1999-2018.
- Boko, M., I. Niang, A. Nyong, C. Vogel, A. Githeko, M. Medany, B. Osman-Elasha, R. Tabo and P. Yanda, 2007: Africa. *Climate Change 2007: Impacts, Adaptation and Vulnerability. Contribution of Working Group II to the Fourth Assessment Report of the Intergovernmental Panel on Climate Change*, M.L. Parry, O.F. Canziani, J.P. Palutikof, P.J. van der Linden and C.E. Hanson, Eds., Cambridge University Press, Cambridge UK, 433-467.

- Brown, J. N., Mearns, R. J., Brown, J. R., & Katzfey, J. (2015). Precipitation projections in the tropical Pacific are sensitive to different types of SST bias adjustment. *Geophysical Research Letters*, 42(24), 10-856.
- Cai, W., Wu, L., Lengaigne, M., Li, T., McGregor, S., Kug, J. S., ... & Ham, Y. G. (2019). Pan-tropical climate interactions. *Science*, 363(6430), eaav4236.
- Chang, P., Fang, Y., Saravanan, R., Ji, L., & Seidel, H. (2006). The cause of the fragile relationship between the Pacific El Niño and the Atlantic Niño. *Nature*, 443(7109), 324.
- Chen, C., Cane, M. A., Wittenberg, A. T., & Chen, D. (2017a). ENSO in the CMIP5 simulations: life cycles, diversity, and responses to climate change. *Journal of Climate*, 30(2), 775-801.
- Chen, L., Li, T., Yu, Y., & Behera, S. K. (2017b). A possible explanation for the divergent projection of ENSO amplitude change under global warming. *Climate Dynamics*, 49(11-12), 3799-3811.
- Chikamoto, Y. (2014). Recent Walker circulation strengthening and Pacific cooling amplified by Atlantic warming. *Nature Climate Change*, 4(10), 888.
- Collins, M., An, S. I., Cai, W., Ganachaud, A., Guilyardi, E., Jin, F. F., ... & Vecchi, G. (2010). The impact of global warming on the tropical Pacific Ocean and El Niño. *Nature Geoscience*, 3(6), 391.
- Dayan, H., Izumo, T., Vialard, J., Lengaigne, M., & Masson, S. (2015). Do regions outside the tropical Pacific influence ENSO through atmospheric teleconnections?. *Climate dynamics*, 45(3-4), 583-601.
- Dee, D. P., Uppala, S. M., Simmons, A. J., Berrisford, P., Poli, P., Kobayashi, S., ... & Bechtold, P. (2011). The ERA-Interim reanalysis: Configuration and performance of the data assimilation system. *Quarterly Journal of the Royal Meteorological Society*, 137(656), 553-597.
- Ding, H., Keenlyside, N. S., & Latif, M. (2012). Impact of the equatorial Atlantic on the El Niño southern oscillation. *Climate dynamics*, 38(9-10), 1965-1972.
- Fathio, I., S. Iizuka, A. Manda, Y.-M. Kodama, S. Ishida, Q. Moteki, H. Yamada, and Y. Tachibana (2017), Assessment of western Indian Ocean SST bias of CMIP5 models, *J. Geophys. Res. Oceans*, 122, 3123–3140, doi:10.1002/2016JC012443. ☐
- Flannaghan, T. J., Fueglistaler, S., Held, I. M., Po-Chedley, S., Wyman, B., & Zhao, M. (2014). Tropical temperature trends in atmospheric general circulation model simulations and the impact of uncertainties in observed SSTs. *Journal of Geophysical Research: Atmospheres*, 119(23), 13-327.
- Fueglistaler, S., Radley, C., & Held, I. M. (2015). The distribution of precipitation and the spread in tropical upper tropospheric temperature trends in CMIP5/AMIP simulations. *Geophysical Research Letters*, 42(14), 6000-6007.
- Gadgil, S., Joseph, V. & Joshi, N. V. Ocean-atmosphere coupling over monsoon regions. *Nature* 312, 141–143 (1984). ☐
- Gadgil, S., & Gadgil, S. (2006). The Indian monsoon, GDP and agriculture. *Economic and Political Weekly*, 4887-4895 ☐

- García-Serrano, J., Cassou, C., Douville, H., Giannini, A., & Doblas-Reyes, F. J. (2017). Revisiting the ENSO teleconnection to the tropical North Atlantic. *Journal of Climate*, *30*(17), 6945-6957.
- Graham, N. E., & Barnett, T. P. (1987). Sea surface temperature, surface wind divergence, and convection over tropical oceans. *Science*, *238*(4827), 657-659.
- Gill, A. E., 1980: Some simple solutions for heat-induced tropical circulation. *Quart. J. Roy. Meteor. Soc.*, **106**, 447–462. □
- Hai-Tien Lee and NOAA CDR Program (2018): NOAA Climate Data Record (CDR) of Monthly Outgoing Longwave Radiation (OLR), Version 2.7. NOAA National Centers for Environmental Information. <https://doi.org/10.7289/V5W37TKD>
- Ham, Y. G., Kug, J. S., Park, J. Y., & Jin, F. F. (2013). Sea surface temperature in the north tropical Atlantic as a trigger for El Niño/Southern Oscillation events. *Nature Geoscience*, *6*(2), 112.
- Ham, Y. G., & Kug, J. S. (2016). ENSO amplitude changes due to greenhouse warming in CMIP5: Role of mean tropical precipitation in the twentieth century. *Geophysical Research Letters*, *43*(1), 422-430.
- He, J., Johnson, N. C., Vecchi, G. A., Kirtman, B., Wittenberg, A. T., & Sturm, S. (2018). Precipitation Sensitivity to Local Variations in Tropical Sea Surface Temperature. *Journal of Climate*, *31*(22), 9225-9238.
- Held, I. M. & Soden, B. J. Robust responses of the hydrological cycle to global warming. *J. Clim.* *19*, 5686–5699 (2006).
- Huffman, G. J., Adler, R. F., Bolvin, D. T., & Gu, G. (2009). Improving the global precipitation record: GPCP version 2.1. *Geophysical Research Letters*, *36*(17).
- IPCC, 2013: Climate Change 2013: The Physical Science Basis. Contribution of Working Group I to the Fifth Assessment Report of the Intergovernmental Panel on Climate Change [Stocker, T.F., D. Qin, G.-K. Plattner, M. Tignor, S.K. Allen, J. Boschung, A. Nauels, Y. Xia, V. Bex and P.M. Midgley (eds.)]. Cambridge University Press, Cambridge, United Kingdom and New York, NY, USA, 1535 pp.
- Izumo, T., Vialard, J., Lengaigne, M., de Boyer Montegut, C., Behera, S. K., Luo, J. J., ... & Yamagata, T. (2010). Influence of the state of the Indian Ocean Dipole on the following year's El Niño. *Nature Geoscience*, *3*(3), 168.
- Izumo, T., Lengaigne, M., Vialard, J., Luo, J. J., Yamagata, T., & Madec, G. (2013). Influence of Indian Ocean Dipole and Pacific recharge on following year's El Niño: interdecadal robustness. *Climate dynamics*, *42*(1-2), 291-310.
- Izumo, T., Vialard, J., Dayan, H., Lengaigne, M., & Suresh, I. (2016). A simple estimation of equatorial Pacific response from windstress to untangle Indian Ocean Dipole and Basin influences on El Niño. *Climate dynamics*, *46*(7-8), 2247-2268.
- Izumo, T., Khodri, M., Lengaigne, M., & Suresh, I. (2018). A subsurface Indian Ocean dipole response to tropical volcanic eruptions. *Geophysical Research Letters*, *45*(17), 9150-9159.

- Jauregui, Y. R., & Takahashi, K. (2018). Simple physical-empirical model of the precipitation distribution based on a tropical sea surface temperature threshold and the effects of climate change. *Climate dynamics*, 50(5-6), 2217-2237.
- Johnson, N. C., and S.-P. Xie, 2010: Changes in the sea surface temperature threshold for tropical convection. *Nat. Geosci.*, 3, 842–845, <https://doi.org/10.1038/ngeo1008>.
- Johnson, N. C., & Kosaka, Y. (2016). The impact of eastern equatorial Pacific convection on the diversity of boreal winter El Niño teleconnection patterns. *Climate dynamics*, 47(12), 3737-3765.
- Jourdain, N. C., Lengaigne, M., Vialard, J., Izumo, T., & Gupta, A. S. (2016). Further insights on the influence of the Indian Ocean dipole on the following year's ENSO from observations and CMIP5 models. *Journal of Climate*, 29(2), 637-658.
- Kanamitsu, M., W. Ebisuzaki, J. Woollen, S-K Yang, J.J. Hnilo, M. Fiorino, and G. L. Potter. NCEP-DOE AMIP-II Reanalysis (R-2). 1631-1643, *Bulletin of the American Meteorological Society*. Nov 2002,
- Khodri, M., Izumo, T., Vialard, J., Janicot, S., Cassou, C., Lengaigne, M., ... & Robock, A. (2017). Tropical explosive volcanic eruptions can trigger El Niño by cooling tropical Africa. *Nature communications*, 8(1), 778.
- Klein, S. A., Soden, B. J., & Lau, N. C. (1999). Remote sea surface temperature variations during ENSO: Evidence for a tropical atmospheric bridge. *Journal of Climate*, 12(4), 917-932.
- Lau, N. C., & Nath, M. J. (2003). Atmosphere–ocean variations in the Indo-Pacific sector during ENSO episodes. *Journal of Climate*, 16(1), 3-20.
- Luo, J. J., Sasaki, W., & Masumoto, Y. (2012). Indian Ocean warming modulates Pacific climate change. *Proceedings of the National Academy of Sciences*, 109(46), 18701-18706.
- McGregor, S., Timmermann, A., Stuecker, M. F., England, M. H., Merrifield, M., Jin, F. F., & Chikamoto, Y. (2014). Recent Walker circulation strengthening and Pacific cooling amplified by Atlantic warming. *Nature Climate Change*, 4(10), 888.
- Merle, J. (1980), Variabilite thermique annuelle et interannuelle de l'Océan Atlantique équatorial Est: L'hypothese d'un "El Niño" Atlantique, *Oceanol. Acta*, 3, 209–220.
- Neelin, J. D., and I. M. Held, 1987: Modeling tropical convergence based on the moist static energy budget. *Mon. Wea. Rev.*, 115, 3–12, [https://doi.org/10.1175/1520-0493\(1987\)115,0003:MTCBOT.2.0.CO;2](https://doi.org/10.1175/1520-0493(1987)115,0003:MTCBOT.2.0.CO;2).
- Ohba M, Ueda H (2005) Basin-wide warming in the equatorial Indian Ocean associated with El Niño. *SOLA*. doi:10.2151/sola
- Parvathi, V., Suresh, I., Lengaigne, M., Izumo, T., & Vialard, J. (2017). Robust projected weakening of winter monsoon winds over the Arabian Sea under climate change. *Geophysical Research Letters*, 44(19), 9833-9843.

- Ramsay, H. A., & Sobel, A. H. (2011). Effects of relative and absolute sea surface temperature on tropical cyclone potential intensity using a single-column model. *Journal of Climate*, 24(1), 183-193.
- Rayner NA, Parker DE, Horton EB, Folland CK, Alexander LV, Row- ell DP, Kent EC, Kaplan A (2003) Global analyses of sea surface temperature, sea ice, and night marine air temperature since the late nineteenth century. *J Geophys Res* 108(D14):4407. doi:10.1 029/2002JD002670
- Reynolds RW, Rayner NA, Smith TM, Stokes DC, Wang W (2002) An improved in situ and satellite SST analysis for climate. *J Clim* 15:1609–1625.
- Richter, I., Xie, S. P., Behera, S. K., Doi, T., & Masumoto, Y. (2014). Equatorial Atlantic variability and its relation to mean state biases in CMIP5. *Climate dynamics*, 42(1-2), 171-188.
- RodríguezFonseca, B., Polo, I., García-Serrano, J., Losada, T., Mohino, E., Mechoso, C. R., & Kucharski, F. (2009). Are Atlantic Niños enhancing Pacific ENSO events in recent decades?. *Geophysical Research Letters*, 36(20).
- Saji, N. H., B. N. Goswami, P. N. Vinayachandran, and T. Yamagata, 1999: A dipole mode in the tropical Indian Ocean. *Nature*, 401, 360–363, <https://doi.org/10.1038/43854>.
- Santoso A, England MH, Cai W (2012) Impact of Indo-Pacific feedback interactions on ENSO dynamics diagnosed using ensemble climate simulations. *J Clim* 25:7743–7763. doi:10.1175/JCLI-D-11-00287.1
- Sobel, A. H., & Bretherton, C. S. (2000). Modeling tropical precipitation in a single column. *Journal of climate*, 13(24), 4378-4392.
- Sobel, A. H., Nilsson, J. & Polvani, L. M. The weak temperature gradient approximation and balanced tropical moisture waves. *J. Atmos. Sci.* 58, 3650–3665 (2001).
- Sobel, A. H., Held, I. M. & Bretherton, C. S. The ENSO signal in tropical 70 tropospheric temperature. *J. Clim.* 15, 2702–2706 (2002).
- Stone, P. H. & Carlson, J. H. Atmospheric lapse rate regimes and their parameterization. *J. Atmos. Sci.* 36, 415–423 (1979).
- Taschetto, A. S., Rodrigues, R. R., Meehl, G. A., McGregor, S., & England, M. H. (2016). How sensitive are the Pacific–tropical North Atlantic teleconnections to the position and intensity of El Niño-related warming?. *Climate dynamics*, 46(5-6), 1841-1860.
- Vecchi, G. A., & Soden, B. J. (2007). Effect of remote sea surface temperature change on tropical cyclone potential intensity. *Nature*, 450(7172), 1066.
- Vecchi, G. A., Swanson, K. L., & Soden, B. J. (2008). Whither hurricane activity?. *Science*, 322(5902), 687-689.
- Vincent, E. M., Lengaigne, M., Menkes, C. E., Jourdain, N. C., Marchesiello, P., & Madec, G. (2011). Interannual variability of the South Pacific Convergence Zone and implications for tropical cyclone genesis. *Climate dynamics*, 36(9-10), 1881-1896.

- Wieners, C. E., Dijkstra, H. A., & de Ruijter, W. P. (2017). The influence of atmospheric convection on the interaction between the Indian Ocean and ENSO. *Journal of Climate*, 30(24), 10155-10178.
- Williams, I. N., & Patricola, C. M. (2018). Diversity of ENSO events unified by convective threshold sea surface temperature: A nonlinear ENSO index. *Geophysical Research Letters*, 45, 9236–9244. <https://doi.org/10.1029/2018GL079203>
- Wittenberg, A. T. (2009). Are historical records sufficient to constrain ENSO simulations?. *Geophysical Research Letters*, 36(12).
- Xie, P. & Arkin, P. A. Global precipitation: A 17-year monthly analysis based on gauge observations, satellite estimates, and numerical model outputs. *Bull. Am. Meteorol. Soc.* 78, 2539–2558 (1997).
- Xie, S. P., Hu, K., Hafner, J., Tokinaga, H., Du, Y., Huang, G., & Sampe, T. (2009). Indian Ocean capacitor effect on Indo–western Pacific climate during the summer following El Niño. *Journal of Climate*, 22(3), 730-747.
- Xie, S. P., Deser, C., Vecchi, G. A., Ma, J., Teng, H., & Wittenberg, A. T. (2010). Global warming pattern formation: Sea surface temperature and rainfall. *Journal of Climate*, 23(4), 966-986.
- Yun, K. S., Yeh, S. W., & Ha, K. J. (2016). Inter-El Niño variability in CMIP5 models: Model deficiencies and future changes. *Journal of Geophysical Research: Atmospheres*, 121(8), 3894-3906.
- Zebiak, S. E. (1993), Air-sea interaction in the equatorial Atlantic region, *J. Clim.*, 6, 1567–1586, doi:10.1175/1520-0442(1993)006<1567:AIITEA>2.0.CO;2.

Figures

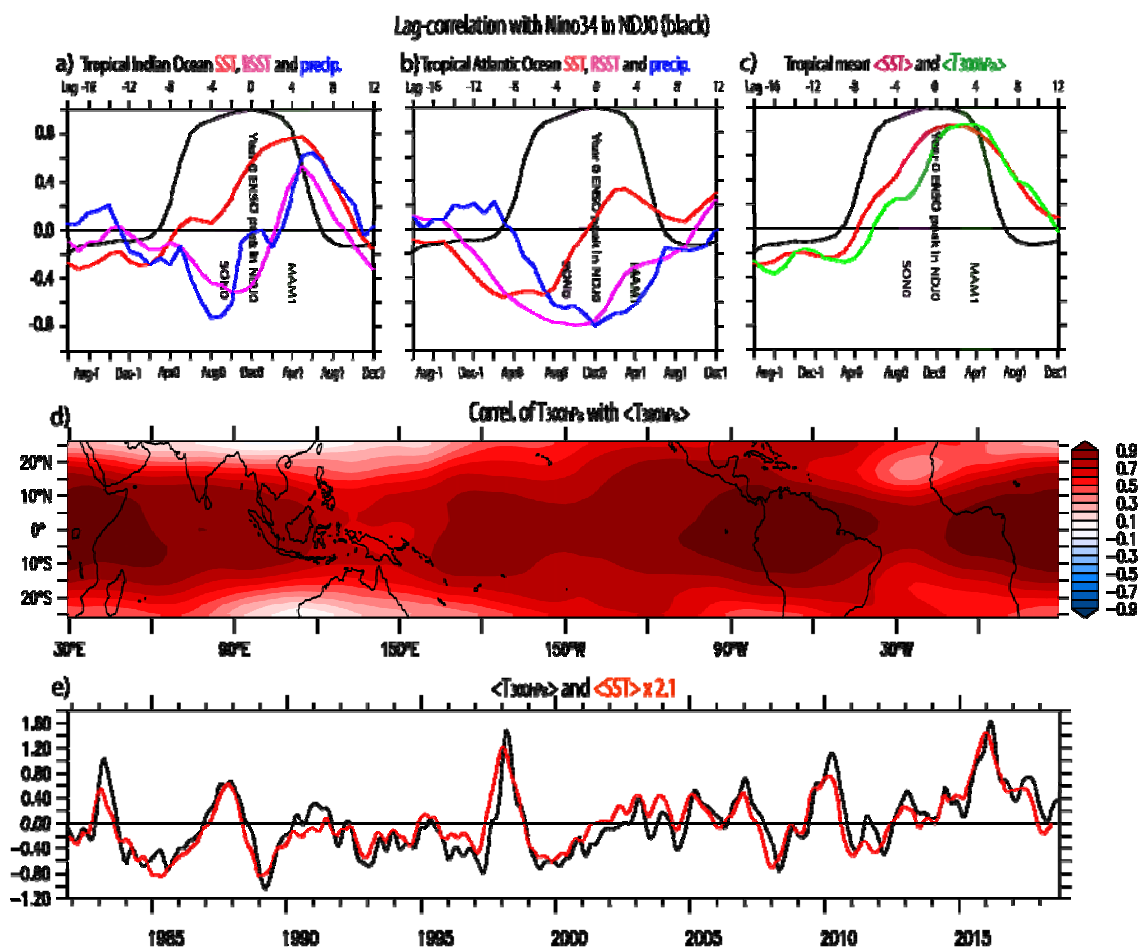


Figure 1. ENSO-induced tropical temperature and precipitation signals. Lag-correlation of November-January of year 0 (NDJ0) Nino3.4 SST anomalies with anomalies of **a)** tropical Indian Ocean (40°E - 110°E , 20°N - 20°S) mean SST (red), relative SST (RSST; SST minus the tropical mean; cyan) and precipitation (blue), **b)** same for tropical Atlantic (70°W - 20°E , 20°N - 20°S), **c)** tropical mean 300 hPa (green) and SST (red). The lagged autocorrelation of Nino3.4 with Nino3.4 in NDJ0 is overlaid in black on panels a, b, c. Vertical shading represent NDJ0, plus SON0 and MAM1 seasons shown in Fig. 3. Panels d, e illustrate the tropical surface and tropospheric signals during ENSO events. **d)** Correlation between 300hPa temperature anomalies and their tropical mean. **e)** Time series of the tropical-mean 300 hPa temperature (black; $^{\circ}\text{C}$) and SST (red; $^{\circ}\text{C}$) anomalies, relative to the monthly climatology. SST anomalies on panel e have been multiplied by 2.1 (value estimated from a linear regression of the 300 hPa Temperature to SST at one month lag, for which the lag-correlation is maximum [not shown], as expected from the equatorial adjustment timescale; e.g. Sobel et al. 2002), i.e. the 300 hPa temperature anomalies are roughly twice larger than the SST anomalies, because of the condensational heating between the wet surface and dry troposphere along the moist adiabatic (as detailed in the online supplementary material; text S2). An intraseasonal smoothing has been applied to all fields (details on the methods in the online supplementary material; text S5).

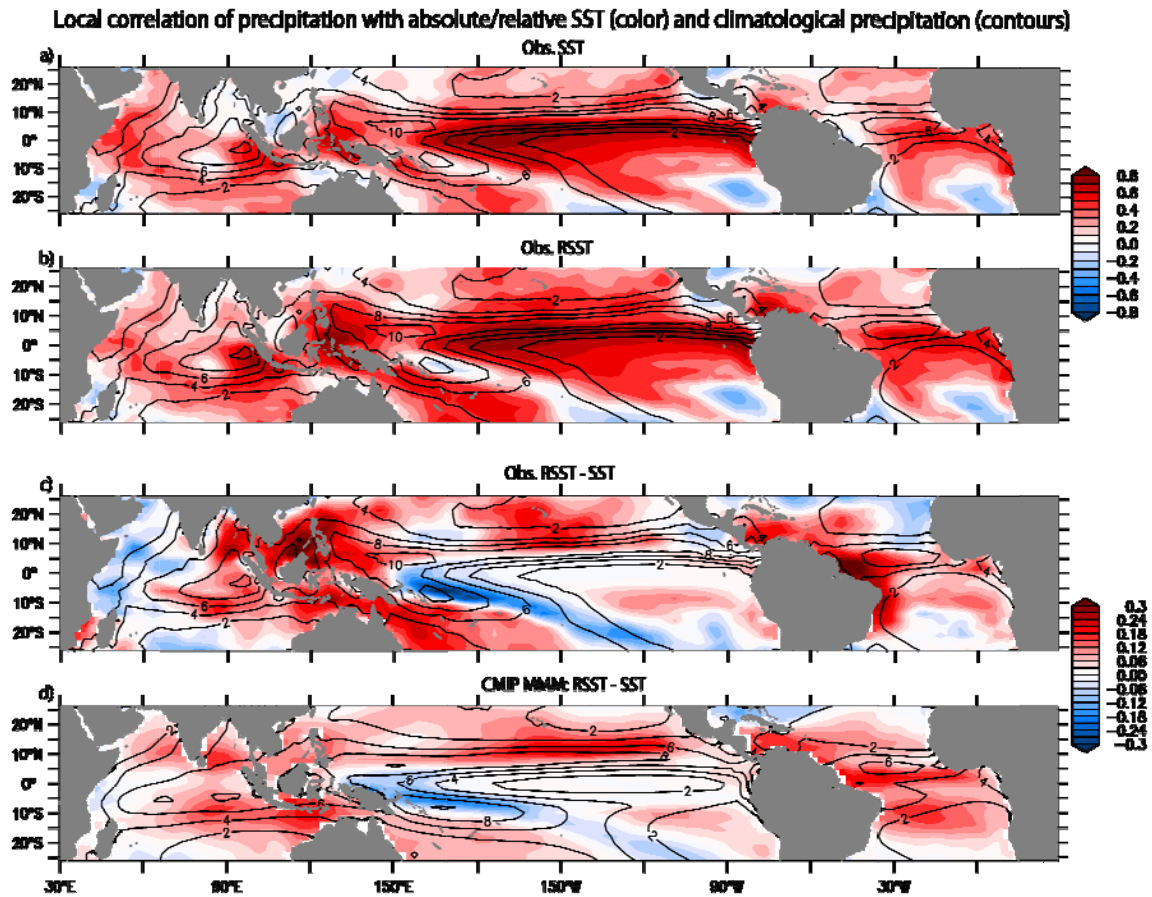


Figure 2. RSST': a more relevant variable for precipitation/deep atmospheric convection interannual variability than SST'. Correlation (color) of observed CMAP precipitation with (a) SST' and (b) RSST'. (c) shows (b) minus (a). The precipitation climatology (mm/day) is overlaid as black contours. (d) as (c), but for the Multi-Model-Mean (MMM) of 36 CMIP climate models (cf. supplementary Figures S3 and S4, and text S3). All anomalies have been low-pass filtered using 5-month time, and 7.5° longitude, Hanning windows, prior to regression. See supplementary figure S1 showing that RSST' explains even better observed outgoing longwave radiation (OLR, a proxy of deep atmospheric convection).

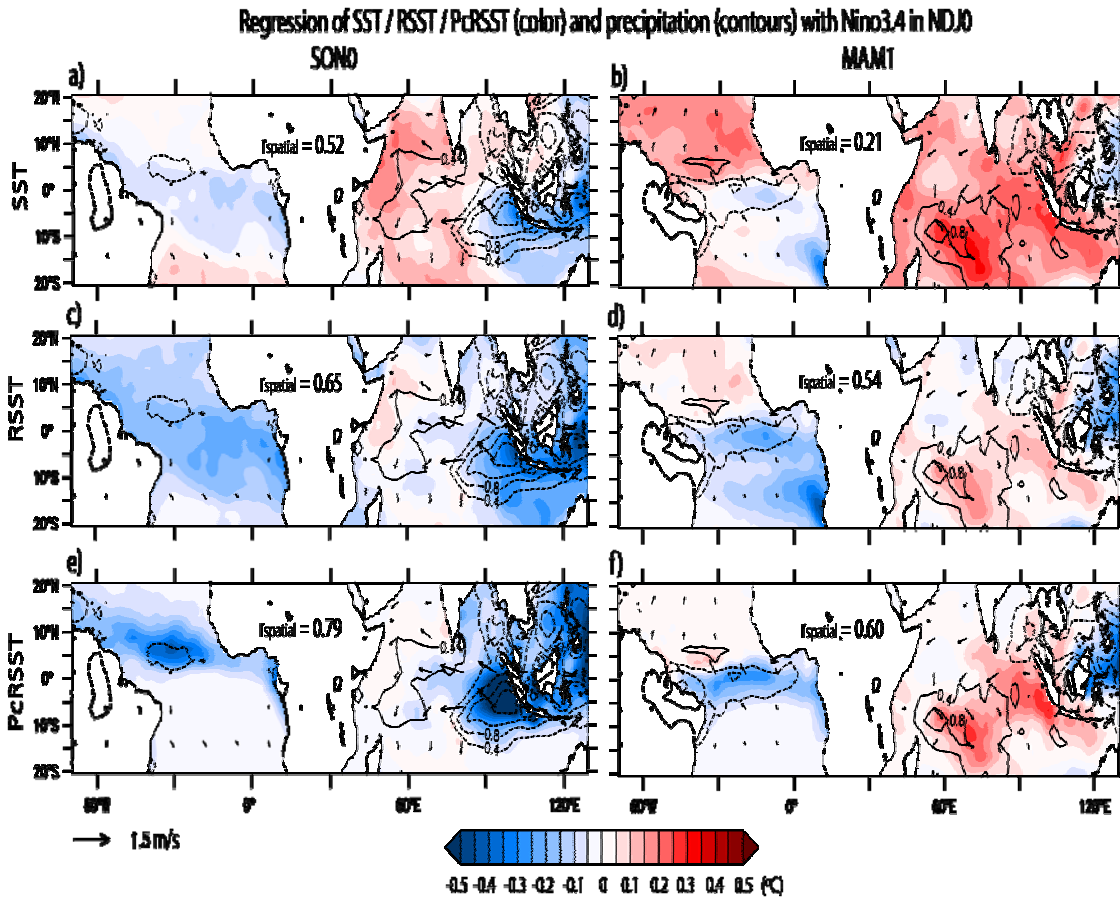


Figure 3. RSST' describe ENSO remote influences on precipitation better than SST'. Seasonally-stratified regression of September-November (SON0) averaged (a) SST' (°C), (c) RSST' (°C) and (e) Climatological precipitation-weighted RSST (PcRSST'; °C) anomalies on the following November to January (NDJ0) Nino3.4 index (normalised by its standard deviation, so that the regression slope illustrates typical amplitudes in physical units). Precipitation (contours; mm day⁻¹) and surface wind (vectors, when significant at the 90% level; at 10 m; m s⁻¹) are overlaid. (b, c, d): Same as a,c,e but for March to May (MAM1) average values regressed onto the preceding November to January (NDJ0) Nino3.4 index. The value of the uncentered spatial pattern correlations (r_{spatial}) between precipitation and SST', RSST' or PcRSST' are indicated on each panel: PcRSST' explains the precipitation anomalies best, followed by RSST'.

Supporting Information for

Relevance of relative sea surface temperature for tropical rainfall interannual variability

Takeshi Izumo^{1,2}, Jérôme Vialard¹, Matthieu Lengaigne^{1,2} and Iyyappan Suresh³

¹ Institut de Recherche pour le Développement, Sorbonne Universités (UPMC, Univ Paris 06)-
CNRS-IRD-MNHN, LOCEAN Laboratory, IPSL, Paris, France

² formerly at Indo-French Cell for Water Sciences, IISc-NIO-IITM-IRD Joint International
Laboratory, NIO, Goa, India

³ CSIR-National Institute of Oceanography, Goa

Contents of this file

Texts S1 to S2

Figures S1 to S7

Texts S3 to S4

Table S1

Text S5

Introduction

The supporting information first presents a complete theoretical derivation of the equations shown in the main text. It then gives figures showing the robustness of the results as well as the CMIP models analysis of historical and projection simulations. It finally gives a detailed description of the data and methods used.

Text S1.

Equations to properly demonstrate why precipitation responds to RSST and PcRSST rather than to SST (and what are the assumptions behind)

A. Derivation of the linear relationship between P' and RSST'

The Gross Moist Stability (GMS; Neelin and Held 1987) can be defined as:

$$\text{GMS} = m_t - m_s \approx m_{300\text{hpa}} - m_s$$

where m is the Moist Static Energy (MSE), $m = s + L_v q = C_p T + g z + L_v q$, s the dry static energy, T the temperature in Kelvin, z the altitude, q the specific humidity (quasi-equal to the mixing vapor ratio in usual conditions), and m_t and m_s respectively the upper tropospheric (at 300hPa, as often used, e.g. Fueglistaler et al. 2015) and surface MSE.

Let us denote $\langle f \rangle$ as the 20°N-20°S tropical mean of any field f , and \bar{f} as the climatological seasonal cycle, and f' as the interannual anomaly, $f' = f - \bar{f}$. Note that, thanks to linearity of these operations, $\langle f' \rangle = \langle f' \rangle$.

The first main assumption is that the mean vertical profile of the tropical atmosphere follows the moist adiabatic lapse rate (**MALR approximation**). Thus, any interannual anomaly $\langle m_s \rangle'$ will lead to the same $\langle m_t \rangle'$ anomaly in the upper troposphere (neglecting the short ~1 month lag in the upper troposphere seen in Fig. 1e), i.e. :

$$\langle m_t \rangle' = \langle m_s \rangle'$$

The second main assumption is that the upper tropospheric temperature interannual anomaly is approximately uniform in the tropics (Weak Tropospheric Gradient approximation; WTG; Sobel et al. 2001), i.e. $T_t' \approx \langle T_t' \rangle$. And, as the upper troposphere is dry, the MSE only depends of temperature (because $m_t \approx s_t = C_p T_{300hPa} + g z_{300hPa} \approx (C_p + R/M_{air}) T_{300hPa}$, assuming air is an ideal gas, R being ideal gas constant and M_{air} being air molar mass), i.e.:

$$m_t' \approx \langle m_t' \rangle$$

Thus, the local GMS interannual anomaly will be:

$$GMS' = m_t' - m_s' \approx \langle m_t' \rangle - m_s' \approx \langle m_s' \rangle - m_s'$$

At the surface, $z_s' = 0$, thus $m_s' = C_p T_s' + L_v q_s'$.

If we assume an almost constant relative humidity, and a 7% °C⁻¹ change in specific humidity (linearization of Clausius-Clapeyron), then $q_s' \approx 0.07 \bar{q}_s T_s'$. Therefore:

$$\begin{aligned} GMS' &\approx \langle (C_p + 0.07 L_v \bar{q}_s) T_s' \rangle - (C_p + 0.07 L_v \bar{q}_s) T_s' \\ &= (C_p + 0.07 L_v \bar{q}_s) (\langle T_s' \rangle - T_s') + 0.07 L_v \mu_{nonlin} \end{aligned}$$

where $\mu_{nonlin} = \langle \bar{q}_s T_s' \rangle - \langle \bar{q}_s \rangle \langle T_s' \rangle - (\bar{q}_s - \langle \bar{q}_s \rangle) T_s'$.

I.e. μ_{nonlin} is a non-linear 2nd order term.

As, by definition, $RSST' = SST' - \langle SST' \rangle = T_s' - \langle T_s' \rangle$, we obtain:

$$GMS' \approx -(C_p + 0.07 L_v \bar{q}_s) RSST' + 0.07 L_v \mu_{nonlin}$$

Thus, GMS' is indeed proportionnal to RSST' if we suppose μ_{nonlin} to be negligible, $|0.07 L_v \mu_{nonlin}| \ll \ll |(C_p + 0.07 L_v \bar{q}_s) RSST'|$, i.e. that the spatial variations of \bar{q}_s are weakly correlated with those of SST' and that \bar{q}_s is close to its tropical mean $\langle \bar{q}_s \rangle$ where SST' is strong (or at least that the two terms within μ_{nonlin} compensate each other). **This is the 3rd main approximation, which has never been discussed before properly to our knowledge.**

And finally, we use Neelin and Held (1987) approximated equation for tropical precipitation (see also He et al. 2018), $P \approx F/GMS$, where F is a constant:

$$P' \approx -(F/\overline{GMS}^2) GMS'$$

$$\Rightarrow P' \approx (F/\overline{GMS}^2) (C_p + 0.07 L_v \bar{q}_s) RSST'$$

We indeed find that temporal anomalies of precipitation should be proportionnal to RSST anomalies, with a factor that should depend of the mean state (of \overline{GMS} and \bar{q}_s), within the limits of the above approximations.

Discussion on the limitations. While this RSST framework seems very robust for climate interannual variability, being relevant in various observational datasets and in almost all of the

CMIP5 models, the approximations highlighted here show that there must be some limitations of the RSST simple approach. RSST, inferred from the thermodynamical constraints on precipitation, is simply defined as $SST - 1 \times \langle SST \rangle$, where the 1 coefficient is fixed. However, the theoretical derivation shows that there are several approximations involved, and that there could be spatial variations in this coefficient related to the climatological mean state and/or to circulation interannual variability effect on precipitation, notably that related to ENSO. A linear regression with two variables, SST and $\langle SST \rangle$, suggests that using a spatially-varying coefficient for $\langle SST \rangle$ could explain even more of precipitation variance (not shown). It suggests that one could increase this coefficient to mimic the larger effect of $\langle SST \rangle$ on atmospheric stability/precipitation in the east Indian Ocean, maritime continent and Northwest tropical Pacific, and in the tropical Atlantic (not shown). This larger effect is likely partly related to ENSO-induced anomalous circulation, with e.g. larger upper-level convergences strengthening drying of these regions during an El Nino (Adames and Wallace 2017). Anyway, RSST framework already explains significantly better precipitation than SST, and keeps the advantage of being simple.

B. Justifying the PcRSST' approach

The previous equation also allows us to justify our PcRSST approach - and to identify the approximation done - to weight RSST' by precipitation climatology \bar{P} , as above equation can be rewritten as:

$$P' \approx \bar{P} RSST' (C_p + 0.07 L_v \bar{q}_s) / \overline{GMS}$$

Thus, our PcRSST approximation supposes that $(C_p + 0.07 L_v \bar{q}_s) / \overline{GMS}$ does not vary too much in the tropics in regions where the product $\bar{P} RSST'$ is non-negligeable, i.e. in regions where it can rain and where RSST' is large. This is obviously a quite crude approximation. Actually, using the approximation that $\bar{P} \approx F / \overline{GMS}$, we could rewrite the above equation as :

$$P' \approx (C_p + 0.07 L_v \bar{q}_s) / F \bar{P}^2 RSST'$$

Knowing that the \bar{q}_s term dominates the first term, and that it is strongly tied to \overline{SST} (relative humidity being quite constant in the tropics), P' might even better match to this more non-linear term: $\overline{SST} \bar{P}^2$. For the sake of simplicity, we have here focussed on the simpler PcRSST concept, as it empirically works and is more intuitive.

Text S2.

Equations to justify the top-heaviness of temperature anomalies

Why do we observe, in observations (Fig. 1e) and all the 36 CMIP models (not shown), that $\langle T_{300hPa} \rangle$ covaries with $\langle SST \rangle$, but with a factor of ~ 2 to 3 ? This top-heaviness for trends as well as for interannual variability has already been noted and explained in earlier studies (e.g. Sobel et al. 2002; Flannaghan et al. 2014, Fueglistaler et al. 2015), but without any proper analytical formulation to our knowledge at present. We here attempt to derive approximate equations justifying this top-heaviness.

Because of the MALR assumption presented in the first appendix, that $\langle m_t \rangle = \langle m_s \rangle$, we can write :

$$(C_p + R/M_{air}) \langle T_{300hPa} \rangle = (C_p + 0.07 L_v \langle \bar{q}_s \rangle) \langle T_s \rangle + 0.07 L_v \beta_{nonlin}$$

where $\beta_{nonlin} = \langle \bar{q}_s T_s \rangle - \langle \bar{q}_s \rangle \langle T_s \rangle$ is a non-linear 2nd order term (the first component of μ_{nonlin} actually), which is negligible if the spatial variations of \bar{q}_s are weakly correlated with those of T_s .

Thus, if we neglect this β_{nonlin} , we indeed have $\langle T_{300hPa} \rangle$ proportionnal to $\langle SST \rangle$:

$$\langle T_{300hPa} \rangle \approx (C_p + 0.07 L_v \langle \bar{q}_s \rangle) / (C_p + R/M_{air}) \langle SST \rangle$$

$$\Rightarrow \langle T_{300hPa} \rangle \approx (1 + 0.07 L_v \langle \bar{q}_s \rangle / C_p) / (1 + R/M_{air}/C_p) \langle SST \rangle$$

with $1 + 0.07 L_v \langle \bar{q}_s \rangle / C_p \approx 1 + [1.8 \text{ to } 3.6]$, if $\langle \bar{q}_s \rangle$ varies between [10 to 20] g/kg and $(1 + R/M_{air}/C_p) \approx 1.3$

Thus, the factor ranges from 2.1 to 3.5 depending of $\langle \bar{q}_s \rangle$, so roughly matching with the observed top-heaviness factor (somewhat overestimating it though).

Discussion on this approximated equation. While this roughly explains the strong control of $\langle SST \rangle$ on $\langle T_{300hPa} \rangle$, we know that there are some limitations to it. Sobel et al. (2002) tried to use “rainy SST” tropical mean (but did not get any statistically significant improvement), and Fueglistaler et al. (2015) used $\langle PSST \rangle$ (precipitation-weighted SST), who show that it explains even more of $\langle T_{300hPa} \rangle$ interannual variance in their models. But in observations and the CMIP coupled models here, we could not find any improvement, e.g. a correlation between the two of 0.89, almost similar to 0.90 when using $\langle SST \rangle$, in observations (consistent with Sobel et al. 2002). Sobel et al. suggested that it may be because of observational issues. However, even in CMIP models for which there are no observational issues, we could not find any improvement (not shown).

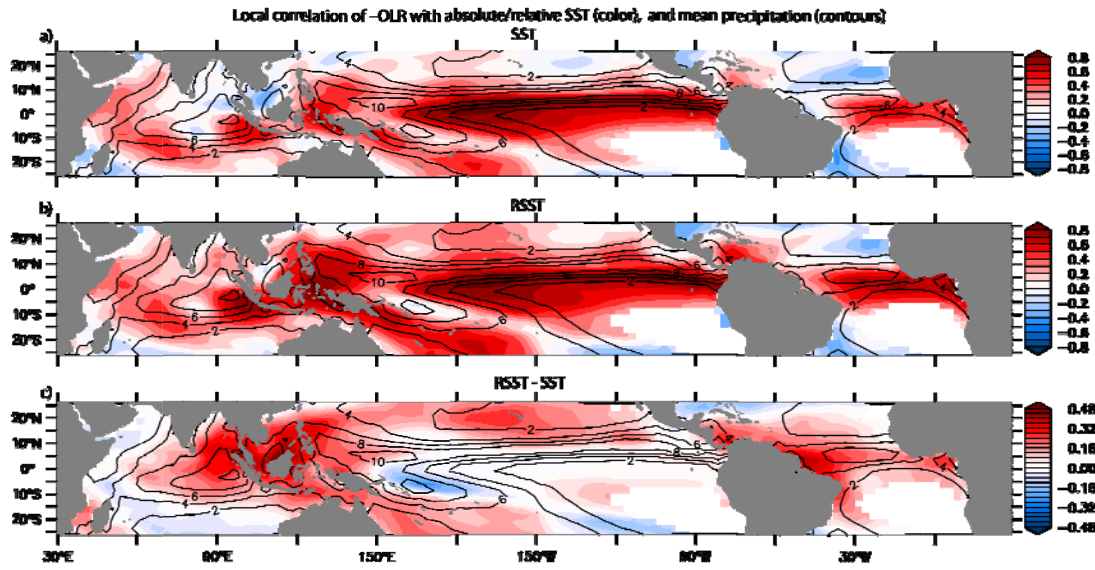


Fig. S1. Improvement thanks to RSST even better when using $-OLR$ (a proxy of atmospheric deep convection). As Fig. 2a,b,c, but using observed outgoing longwave radiation (OLR) anomalies multiplied by -1 , instead of CMAP1 precipitation dataset. Here dry regions (CMAP1 precipitation climatology $< 0.5\text{mm/day}$), where OLR is not anymore a good proxy of deep convection/precipitation, are masked. This figure shows generally similar results (with only a few differences especially in climatologically drier regions, e.g. subtropical Pacific and Atlantic oceans, and tropical west Indian Ocean and east Atlantic), but with a larger amplitude of the improvement thanks to RSST (panel c; note that its color scale is much larger than in Fig. 2c), possibly because OLR is a better observed and more homogeneous satellite-based dataset than precipitation and because it represents more convective precipitation anomalies.

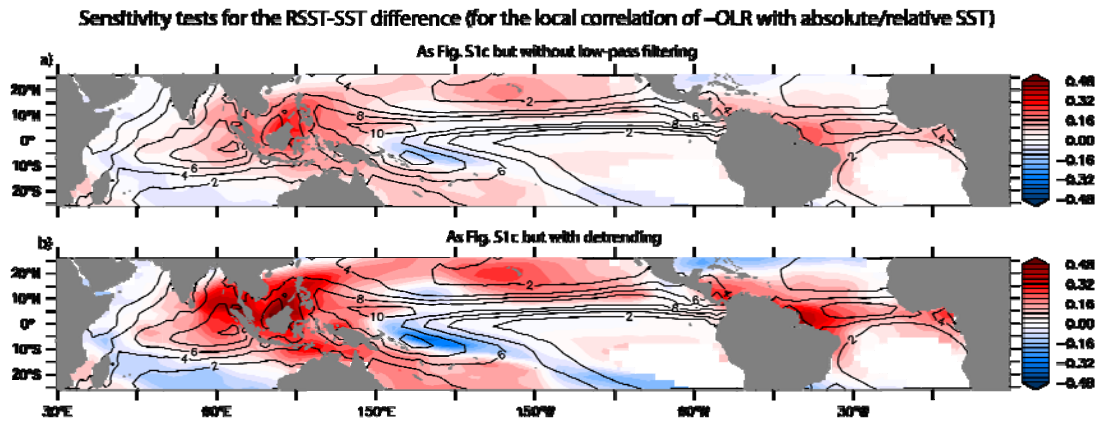


Fig. S2. Robustness of RSST-SST difference in local correlation between deep convection and SST/RSST when removing intraseasonal filtering or when detrending. **a** as Fig. S1c, but for raw monthly data without the low-pass intraseasonal 5-month Hanning filter. **b** as Fig. S1c, but with a linear detrending applied. The RSST-SST difference in local correlation is still positive in most regions (even without low-pass filtering when intraseasonal noise weakens correlations; detrending leads only to small changes), emphasizing the results robustness.

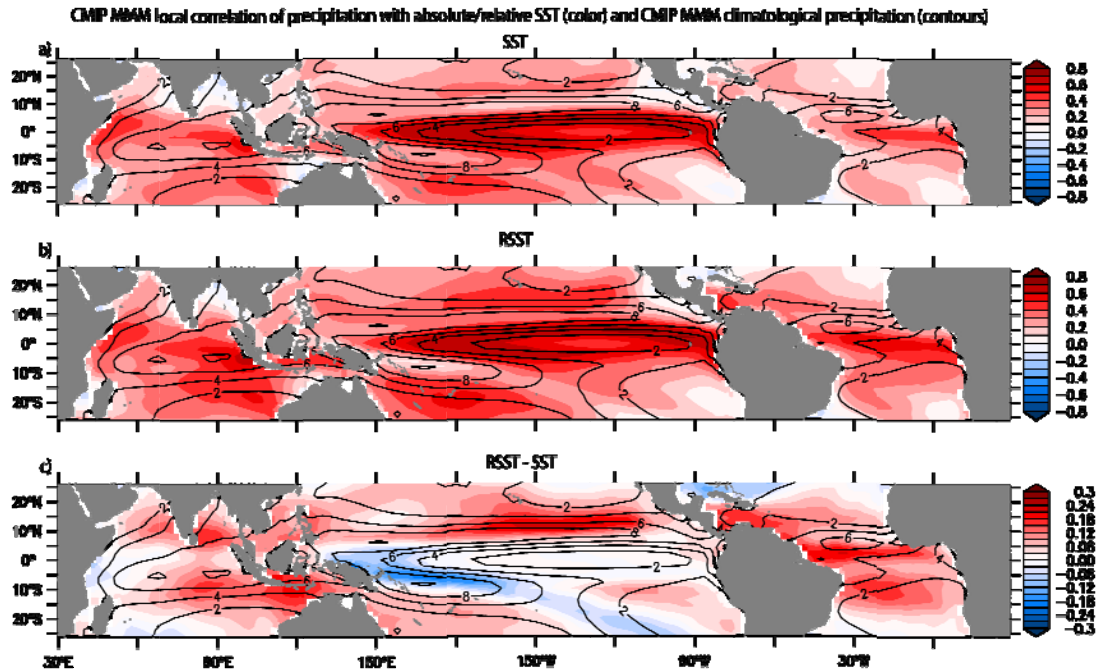


Fig. S3. Robustness of the local correlations shown on Fig. 2abc when using CMIP Multi-Model-Mean (MMM; 36 models). As Fig. 2a,b,c, but for CMIP5 MMM (last 30 years of historical runs; cf. supplementary textS3; panel c here is the same as Fig. 2d).

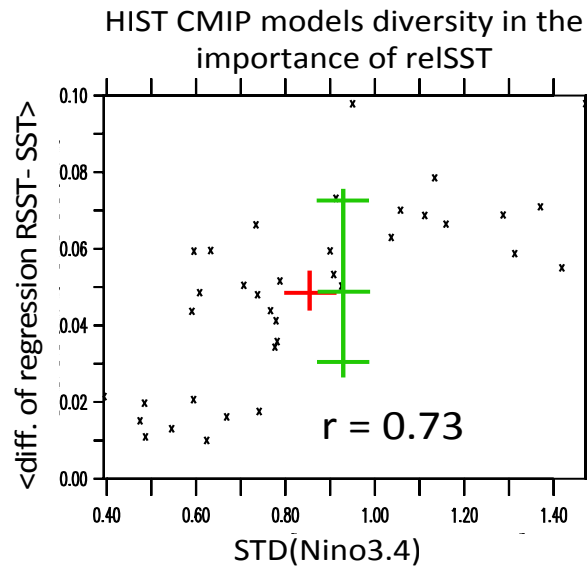


Fig. S4. Relevance of relative SST in CMIP5 models and inter-model diversity. Inter-model diversity in the added value of using RSST instead of SST (vertical axis) well explained by the diversity in ENSO amplitude (measured as the STD of Nino3.4 SST ; horizontal axis). The added value of RSST is defined as the tropical mean of the regression slopes difference RSST-SST (regression associated to the correlation in Fig. S3; unit: mm/day per STD of RSST or SST, to have typical amplitudes). MMM (red crosses) and inter-model correlation given for both panels. 1981-2018 observed values have been added for three different precipitation estimates to highlight observed uncertainties on precipitation amplitudes (uncertainties much weaker for SST ; not shown), in increasing order : GPCPv2.3, CMAP1 (used all along this study) and scaled OLR (i.e. large

uncertainties among precipitation estimates, lower for GPCP, larger for scaled OLR). See supplementary text S3 for details.

Regression of SST / RSST / PcRSST (color) and precipitation (contours) with Nino3.4 in NDJ0

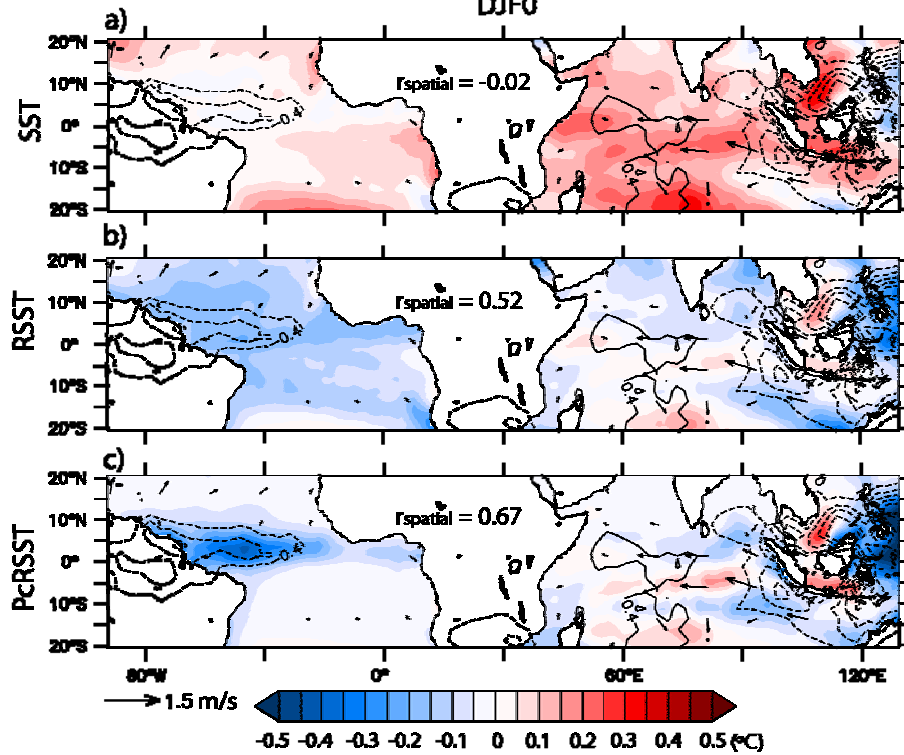


Fig. S5. As Fig. 3b but for DJF0 (December-February during ENSO peak). Using RSST, and even more PcRSST, leads to a much better match than using SST, also for DJF0, notably in the tropical Atlantic to explain the drying effect on west equatorial Atlantic and South America.

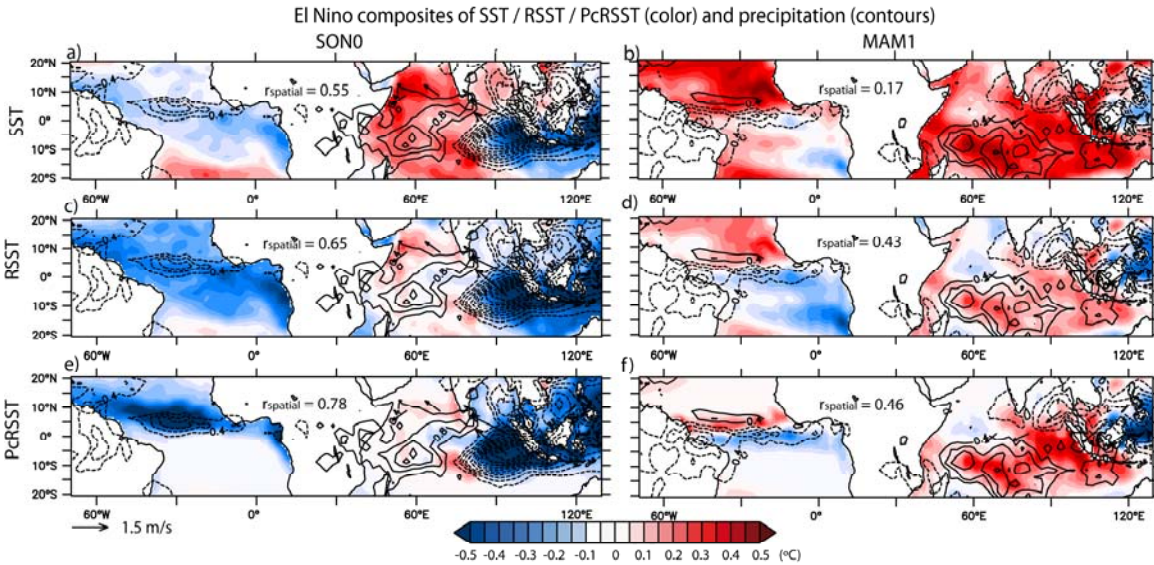


Fig. S6. As Fig. 3 but for El Niño composites. El Niño events are defined when Niño3.4 SSTA in NDJ exceeds 2/3 of its standard deviation (10 events during the 1981-2018 period). RSST and PcRSST outperform SST in explaining El Niño precipitation teleconnections as quantified by the pattern correlation between precipitation and PcRSST/RSST/SST anomalies shown on each panel.

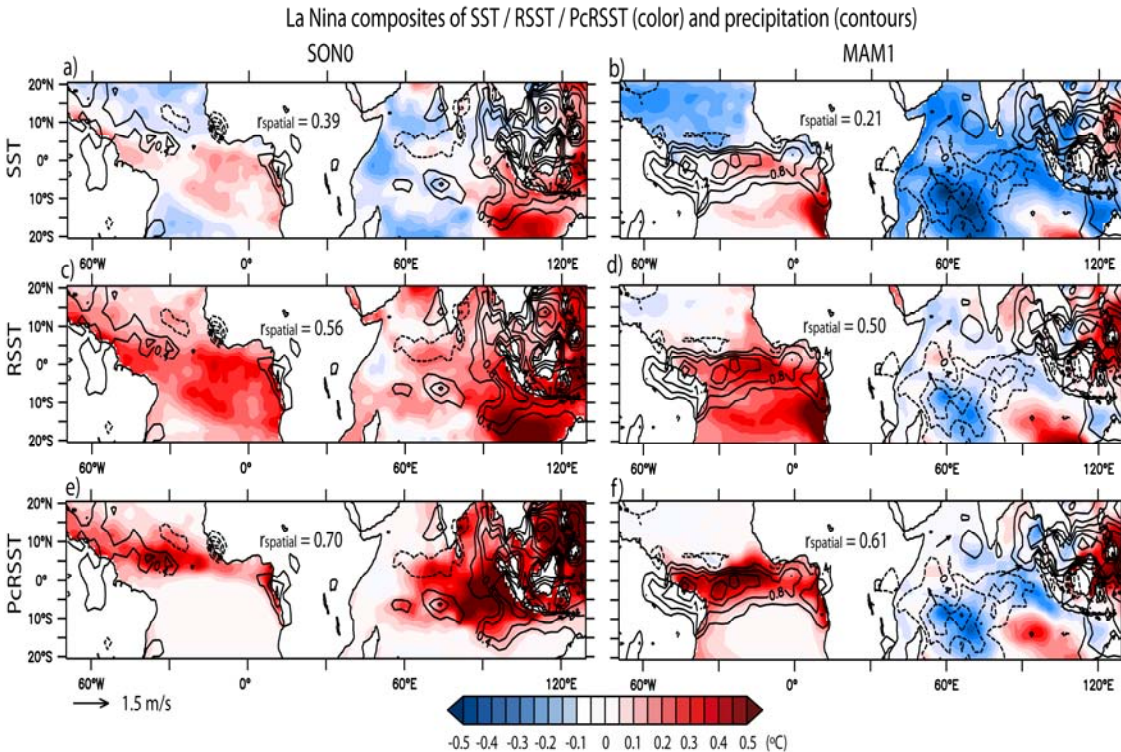


Fig. S7. As Fig. S6 but for La Niña composites. La Niña are defined when Niño3.4 SSTA in NDJ drops below -2/3 STD (10 events during the 1981-2018 period). As for El Niño, RSST and PcRSST outperform SST in explaining La Niña precipitation teleconnections as quantified by the pattern correlation between precipitation and PcRSST/RSST/SST anomalies on each panel.

Text S3.

Historical CMIP analyses

Climate models are essential to understand processes, to have longer time series without observational issues, and to be able to estimate future changes due to climate change. Thus, verifying that our observations-based results remain valid in CMIP5 historical runs, and trying to understand the potential inter-model diversity in the relevance of RSST, is crucial.

CMIP models description. Here we use the same 36 CMIP5 models (IPCC, 2013) as in Parvathi et al. (2017), for which we had SST and precipitation available (Suppl. Table S1). Models having the advantage of having no observational uncertainty on precipitation, we have directly analysed precipitation instead of OLR. Historical runs being available usually for 1861-2005 period, results are shown for the last 30 years, i.e. 1976-2005, to be roughly comparable to the 1981-2018 period (results being almost similar when using the full historical period; not shown). All outputs were re-gridded to a 2° regular grid. We show only the Multi-Model Mean (MMM), for the sake of simplicity (checking that results inferred from MMM remain mostly valid for each model; not shown; see also Fig. S4). We acknowledge the World Climate Research Program's Working Group on Coupled Modelling, which is responsible for CMIP, and we thank the climate modeling groups (listed in Table S1) for producing and making available their model outputs. All the CMIP5 model outputs were downloaded from the Institut Pierre Simon Laplace (IPSL) CICALAD repository.

Confirming observations-based results with CMIP historical runs. Given the observational uncertainties related to the limited length of the record and measurement errors, we performed similar analyses to observations-based ones in our 36 CMIP5 historical simulations. Our results indicate that the CMIP5 models realistically simulate the strong relationship between $\langle \text{SST} \rangle$ and $\langle T_{300\text{hPa}} \rangle$ interannual variations, with a Multi-Model Mean (MMM) maximum correlation of 0.77 (ranging from ~ 0.6 to ~ 0.9 for individual models) at ~ 1 month lag and a similar amplitude ratio between $\langle \text{SST} \rangle$ and SST (ranging from ~ 1.9 to ~ 2.6). CMIP5 models also display a pattern of SST-precipitation relationship (Suppl. Fig. S3a) qualitatively consistent with that shown on Fig. 2a and Fig. S1a for observations). As in observations, RSST better explains deep convection/rainfall interannual variability than SST. The improvement of the local correlation is however smaller than in observations (Figure S3abc vs Figures 2abc and S1abc). Although broadly located in the same areas as in observations, the improvement pattern displays biases that are reminiscent of CMIP5 model climatological biases, including a degradation over the western equatorial Pacific that generally hosts a prominent cold tongue bias, a weaker improvement over the eastern equatorial Indian Ocean in line with the positive IOD-like mean state bias. And, keeping in mind that the relationships with precipitation should be generally larger in climatologically-rainy regions (cf. PcRSST concept), these MMM maps have biases in their spatial patterns expected from models typical biases, notably the well-known double ITCZ / cold tongue bias in the tropical Pacific (e.g. Bellenger et al. 2014; Brown et al. 2015), the positive IOD-like mean state bias in the IO (e.g. too strong/weak precipitation in the west/east equatorial IO related to SST gradient bias ; e.g. Fathrio et al. 2017) and Atlantic Nino-like bias in the Atlantic (e.g. Richter et al. 2014). Also, the spatial patterns and amplitudes, while qualitatively agreeing, vary among models (not shown), as their biases do. To quantify the inter-model diversity in the importance of RSST, we define a simple metrics : the tropical mean of the increase, when using RSST instead of SST, of the slope of the regression (of precipitation onto normalised SST or RSST). We also use the STD of Nino3.4 SST as a measure of ENSO amplitude, whose inter-model diversity is large in CMIP (e.g. Bellenger et al. 2014), and explains the diversity in $\text{STD}(\langle \text{SST} \rangle)$: intermodel correlation $r=0.80$ between $\text{STD}(\langle \text{SST} \rangle)$ and $\text{STD}(\text{Nino3.4})$. Thus we find the following expected relationship: the larger the amplitude of ENSO, and thus of $\langle \text{SST} \rangle$, the larger the importance of relative SST in the model ($r=0.73$). This diversity is important, $\text{STD}(\text{Nino3.4})$ ranging from ~ 0.4 to $\sim 1.5^\circ\text{C}$, and the increase in $\langle \text{slope} \rangle$ ranging from ~ 0.01 to ~ 0.1 mm/day per STD (Suppl. Fig. S4). The MMM is roughly consistent, for this regression slope-based

metrics, when averaged over the whole tropics, with CMAP1 observations (Suppl. Fig. S4). To conclude, CMIP historical simulations confirm the usefulness of RSST, with nevertheless some expected biases and a large inter-model diversity, models having too weak ENSO (and thus $\langle \text{SST} \rangle$) variability having difficulties to simulate this importance of RSST. These results should remain valid in the following CMIP6 phase, with hopefully some improvements thanks to potentially-reduced biases (e.g. cold tongue bias).

Text S4.

CMIP projected changes driven by ENSO projected changes

Since CMIP models in general reasonably capture the RSST role, it is worth investigating potential projected changes in this RSST role. So we also analysed RCP8.5 projection runs, available over the 2006-2099 period.

Methods. We chose the unmitigated RCP8.5 scenario because of the larger forcing, and so larger signal/noise ratio, and also because it is the scenario that is up to present – unfortunately - the most realistic. Future changes due to anthropogenically-forced climate change are defined for each model as the difference between the last 30 years of RCP8.5 minus the last 30 years of historical simulation. We did robustness tests by using instead 50-year long period, or by choosing different 30-year periods. E.g. we have checked that the changes in $\text{STD}(\text{Nino3.4})$ are not purely random (i.e. not only due to aliasing of internal variability when computed over 30 years period, e.g. Wittenberg 2009): if the changes in $\text{STD}(\text{Nino3.4})$ are computed using a different choice of 30 years periods (i.e. 2040-2069 minus 1946-1975 instead of 2070-2099 minus 1976-2005), then the intermodel correlation between the changes in $\text{STD}(\text{Nino3.4})$ for these two choices of periods is 0.65, hence significantly positive at the 99.9% level.

MMM projected changes. The projected warming trend is so large in the last 30 years of the 21st century in RCP8.5 runs that it reduces the local relationship of precipitation with SST for that future 30-year period (precipitation having a weaker and less spatially-homogeneous trend than SST; e.g. Held and Soden 2006; Xie et al. 2010). Such effect of the trend is much weaker in the historical last 30 years (not shown). Hence, as this global warming trend is by construction absent in RSST, there is a clear increase in the added value of RSST for most models (positive in 35 out of 36 models, ranging from about -0.02 to +0.16 mm/day per STD, using the metrics used in Fig. S4; not shown). This increase of the added value of RSST is only due, for the MMM, to this trend increase from historical to RCP8.5 last 30 years. If the above analysis is redone after detrending all variables for each 30-year period separately, the sign of the projected change varies among models, and is negligible for the MMM.

Diversity in projected changes. Actually, earlier studies have shown a large diversity among CMIP models in the debated projected change of ENSO variance (e.g. Collins et al. 2010, Ham and Kug 2016 ; Yun et al. 2016 ; Chen et al. 2017a,b). From the above historical runs results, we expect this diversity to project onto the $\text{STD}(\langle \text{SST} \rangle)$ changes, and thus on the changes in RSST importance. Indeed, the $\text{STD}(\langle \text{SST} \rangle)$ changes in RCP8.5 scenario are strongly related to the $\text{STD}(\text{Nino3.4})$ changes ($r=0.80$; correlations in this paragraph given for detrended variables to only focus on interannual variability projected changes). Hence, RSST becomes more important in the models which project an increase in ENSO amplitude ($r=0.72$) and of $\langle \text{SST} \rangle$ ($r=0.87$). The diversity in the projected change is large, from about -0.03 up to $\sim +0.04$, relatively to the ~ 0.05 (mm/day per STD) historical MMM value.

Conclusion. To conclude this CMIP analysis, it confirms the relevance of the RSST framework. This RSST relevance is qualitatively robust, and is projected to remain robust in the future - and will be even more helpful because of increasing trend issues - in all our CMIP database,

and is larger in models with larger ENSO amplitude. CMIP results are however obviously affected by some typical CMIP5 biases, e.g. the double ITCZ/cold tongue bias, and by the uncertainties in ENSO amplitude projections.

Institut	Model
BCC	bcc-csm1-1
	bcc-csm1-1-m
BNU	BNU-ESM
CCCma	CanESM2
CMCC	CMCC-CESM
	CMCC-CMS
CNRM-CERFACS	CNRM-CM5
CSIRO-BOM	ACCESS1-3
CSIRO-QCCCE	CSIRO-Mk3-6-0
FIO	FIO-ESM
IPSL	IPSL-CM5A-LR
	IPSL-CM5A-MR
	IPSL-CM5B-LR
LASG-CESS	FGOALS-g2
LASG-IAP	FGOALS-s2
MIROC	MIROC5
	MIROC-ESM
	MIROC-ESM-CHEM
MOHC	HadGEM2-CC
MPI-M	MPI-ESM-LR
	MPI-ESM-MR
MRI	MRI-CGCM3
	MRI-ESM1
NASA-GISS	GISS-E2-H
	GISS-E2-H-CC
	GISS-E2-R
	GISS-E2-R-CC
NCAR	CCSM4
NCC	NorESM1-M
	NorESM1-ME
NIMR-KMA	HadGEM2-AO
NOAA-GFDL	GFDL-CM3
	GFDL-ESM2G
	GFDL-ESM2M
NSF-DOE-NCAR	CESM1-BGC
	CESM1-CAM5

Table S1. List of the 36 CMIP5 models used.

Text S5.

Data and Methods

A. Methods.

Relative SST is defined as the SST minus $\langle \text{SST} \rangle$, the latter being 20°N-20°S average SST (as in Johnson and Xie 2010). As earlier studies by e.g. Vecchi and Soden 2007 had used 30°N-30°S, we did some robustness tests with 15°N-15°S, 25°N-25°S, 30°N-30°S: we obtain similar results qualitatively, with larger differences to absolute SST if 15°N-15°S is used (because then $\text{STD}(\langle \text{SST} \rangle)$ is larger), and vice versa weaker if 30°N-30°S is used, the best match with precipitation being generally around 20°N-20°S (not shown).

We use classical indices of interannual tropical climate modes during their peak seasons, such as the November to January (NDJ) Niño3.4 (170°W-120°W; 5°N-5°S) SST anomalies index in for ENSO, the Dipole Mode Index (DMI, defined as average SST anomalies difference over 50°E-70°E; 10°N-10°S minus those over 90°E-110°E; 0°-10°S; and its west and east poles separately, either using SST or RSST) averaged from September to November (SON) for the Indian Ocean Dipole following Saji et al. (1999) and Atl3 (20°W-0°, 3°N-3°S; cf. Zebiak et al. 1993) SST anomalies averaged over April to June (AMJ) for the Atlantic Niño (since it peaks in may; Munchen and Neelin). For lag-correlation/regression with NDJ0 Niño3.4 SST, the year number is by convention the year of the first month of the three months average (e.g. MAM1 is following March-May period). Intraseasonal variability is smoothed out using a 5-months Hanning low-pass filter. To estimate the statistical significance, we compute the effective number of degrees of freedom when all seasons are mixed (formulae 30 of Bretherton et al. 1999), and one degree of freedom per year for seasonally-stratified analyses. We use the usual two-tailed Student t-test to test whether Pearson correlation and linear regression are significantly different from 0 or not. Steiger's Z test is used to test the significance of the difference in correlation. We compute uncentered pattern correlation (r_{spatial}), more suited here than centered pattern correlation, i.e. spatial means are not removed, between precipitation and e.g. SST anomalies. The intraseasonal variability (e.g. the Madden-Julian Oscillation) is smoothed out with a 5 months Hanning filter to remove signals with periods less than ~3-4 months.

B. Observational datasets

This paper uses the OISSTv2 monthly product (Reynolds et al. 2002) for SST available since November 1981 (we also used HadiSST [Rayner et al. 2003] to verify the robustness of the results) and NCEP2 reanalysis (Kanamitsu et al. 2002) for upper tropospheric temperature at 300hPa $T_{300\text{hPa}}$. We use Climate Data Record (CDR) Outgoing Longwave Radiation (OLR) v2.7 from NOAA (Hai-Tien Lee and NOAA CDR Program 2018) as a proxy for deep atmospheric convection, given the large uncertainties in the existing rainfall products. As a comparison to the monthly CMAP1 precipitation product mainly shown all along this paper, we also verified that the results are robust (not shown; see also comparison in Fig. S4) when using GPCPv2.3 product (Huffman et al. 2009), when using a « scaled OLR » precipitation product (in which we multiplied OLR anomalies by the regression slope from the regression of CMAP1 precipitation onto OLR; Fig. S4) or when using the former NOAA interpolated OLR product. We also use ECMWF ERAI atmospheric reanalysis (Dee et al. 2011) wind at 10m for Figures 3, S5, S6 and S7. All analyses are made over the November 1981 (from which OISSTv2 is available) to 2018 period.